The structure of indium phosphide (001) treated with trimethylantimony in a metalorganic vapor-phase epitaxy reactor

Y. Sun, S. F. Cheng, G. Chen, R. L. Woo, and R. F. Hicks[a)]
Chemical Engineering Department, University of California, Los Angeles, California 90095

(Received 10 November 2004; accepted 4 March 2005; published online 4 May 2005)

Indium phosphide (001) surfaces were exposed to 0.61-mTorr trimethylantimony in a metalorganic vapor-phase epitaxy reactor. The antimony surface composition increased rapidly with dosage and saturated at 22.0 at. % for temperatures between 450 and 600 °C. The results indicate that a thin layer of InSb formed on the surface, ~6.8 Å thick. Strain from the lattice mismatch caused faceting in the [110] direction, whereas the formation of Sb dimer bonds relieved the strain in the [−110] direction. As a result, narrow ridges formed that ranged from 4 to 10 nm wide and from 3.0 to 18.0 Å high, depending on the antimony coverage. © *2005 American Institute of Physics*. [DOI: 10.1063/1.1897485]

I. INTRODUCTION

Antimonide-based materials on indium phosphide have attracted attention due to their potential device applications. The type-II band alignment between InP and GaAsSb and the narrow band gap energy of GaAsSb make it well suited for the base layer in heterojunction bipolar transistors.[1–3] In addition, antimony can act as an electrical passivation layer for InP,[4–6] and as a surfactant in the epitaxial growth process.[7–9]

Metalorganic vapor-phase epitaxy (MOVPE) is widely used to fabricate III/V compound semiconductors containing antimony and phosphorus.[10–14] During the growth of heterojunctions, e.g., GaAsSb on InP, the group-V source must be switched from phosphorus to antimony and arsenic. The lack of common elements in this material system makes the heterojunction growth challenging, as simultaneous adsorption, desorption, and bulk diffusion of antimony, arsenic, and phosphorus may occur, leading to intermixing at the interface.[15] Precise switching procedures and growth interruptions are used to control these phenomena, but they have been met with limited success.[16–19] Cross-sectional transmission electron micrographs have shown that GaAsSb/InP superlattices exhibit a diffuse and strained interface for GaAsSb growth on top of InP.[11,12]

In this work, we have characterized InP (001) surfaces that have been exposed to trimethylantimony (TMSb) in a MOVPE reactor at 450–600 °C. The antimony quickly saturates the surface and does not appear to diffuse into the bulk crystal. The strain induced by Sb adsorption leads to faceting, and the formation of narrow ridges, 4–10 nm in width, that extend along the [−110] direction.

II. EXPERIMENTAL METHODS

Indium phosphide films, 0.10 μm thick, were grown on *n*-type, vicinal InP (001) substrates in a Veeco D125 MOVPE reactor. The reactor was maintained at 60 Torr with a total flow of 37.0-standard-liter/min ultrahigh-purity hydrogen. The H_2 was passed through a SAES Pure Gas, Inc. purifier (model PS4-MT3-H) which removed any remaining oxygen, nitrogen, or carbon species to below a few ppb. Antimony was dosed onto the indium phosphide surface by exposing the crystal to 6.1×10^{-4} Torr of TMSb at 450–600 °C for 10–600 s. After exposure, the samples were cooled to 30 °C in a H_2 ambient at a rate of 1 °C/s.

After the TMSb exposure, the samples were analyzed by x-ray photoelectron spectroscopy (XPS), low-energy electron diffraction (LEED), and scanning tunneling microscopy (STM). Core-level photoemission spectra of the Sb 3*d*, P 2*p*, and In 3*d* lines were collected by a PHI 3057 XPS spectrometer, using aluminum $K\alpha$ x rays ($h\nu$=1486.6 eV). All spectra were taken in small area mode with a 7° acceptance angle and 23.5-eV pass energy. The takeoff angle with respect to the surface normal was 25°. The STM micrographs were obtained using a Park autoprobe/VP scanning tunneling microscope. The sample bias was −2.8 V and the tunneling current was 0.5 nA.

III. RESULTS

Shown in Fig. 1 is a scanning tunneling micrograph for an InP (001) film, 0.1 μm thick, after transferring the sample from the MOVPE reactor to the ultrahigh-vacuum (UHV) system. The surface contains atomically flat terraces with an average width of 80 nm. This terrace width corresponds to a substrate miscut of ~0.2°. The step edges are not straight because the miscut orientation is 8.3° away from the [110] direction as detected by x-ray diffraction. A sharp (2×1) low-energy electron-diffraction pattern is exhibited by this surface, indicating that it is well ordered.[20]

Dosing the indium phosphide surface with TMSb led to a rapid increase in the antimony coverage on the surface. Shown in Fig. 2 is the dependence of the Sb at. % on the exposure time and temperature. The Sb at. % is determined from the integrated intensities of the Sb 3*d*, In 3*d*, and P 2*p* peaks, excluding C 1*s* and O 1*s* peaks which were small. A rapid uptake of antimony was recorded over the first 50 s, after which the coverage remained constant at 22.0 at. %. For all the temperatures studied, the uptake curves are the

[a)]Author to whom correspondence should be addressed; electronic mail: rhicks@ucla.edu

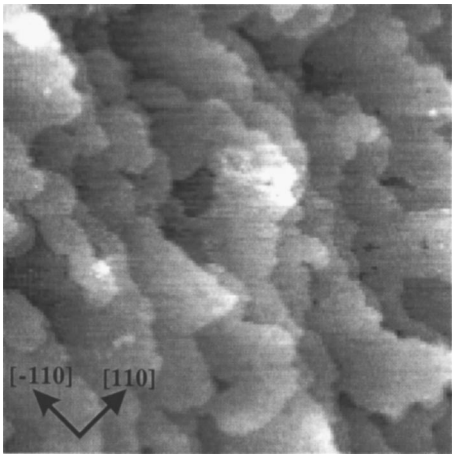

FIG. 1. Scanning tunneling micrograph of the clean InP (001) surface (image size=0.6×0.6 μm^2).

same to within experimental error. Note that it takes only 2.5 s for the reactor to respond to a step change in the inlet feed composition.

Listed in Table I are the at. % of In, P, and Sb atoms in the near surface region following exposure to different doses of TMSb. The Sb/In ratio is shown in column 4. The trend in the changes of these numbers is the same as those of Sb at. %, since In at. % varies only slightly. To convert from Sb at. % into Sb/In ratio, multiply the former value by 1.96 ± 0.07. The P/In ratio is also tabulated in column 5. It is seen that this ratio decreases monotonically as Sb adsorption increases. Evidently, the Sb replaces the P in the topmost layers of the crystal.

After covering the InP (001) surface with 22.0 at. % Sb, a streaky $(2\times n)$ LEED image is obtained, as shown in Fig. 3(a). This picture was taken after exposure to TMSb for 90 s at 500 °C in the MOVPE reactor. All the antimony-treated samples have a LEED pattern similar to the one shown in the figure. No other lattice structures were observed. There are faint half streaks in the [−110] direction and the diffraction spots in the [110] direction are diffused and distributed unevenly. The spacing between spots ranges from 1/6 to 1/3 of the reciprocal-space lattice. For comparison, the LEED picture for an In-rich InP $(001)-(2\times4)$ surface is presented in Fig. 3(b). This structure is obtained after annealing a clean InP crystal in H_2 for 90 s at 500 °C. It is seen that the $\times4$ spots are clearly discerned as opposed to those found in Fig. 3(a). Note that the dashed boxes correspond to the (1×1) reciprocal-space lattice.

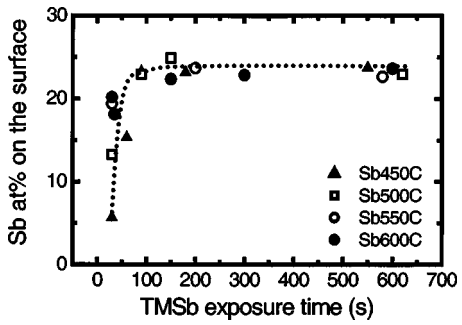

FIG. 2. The dependence of the antimony uptake on time and temperature of exposure to 0.61-mTorr TMSb, corresponding to 610 L/s.

TABLE I. Composition of the InP surface after different TMSb exposures, excluding carbon and oxygen.

Sb at. %	In at. %	P at. %	Sb/In	P/In
0.0	53.5	46.5	0.0	0.87
5.4	52.8	41.8	0.10	0.79
10.8	51.9	37.3	0.21	0.72
14.1	51.1	34.8	0.28	0.68
22.0	48.1	29.9	0.46	0.62

In the following paragraphs, the morphological evolution of the film will be examined by scanning tunneling microscopy. It was found that the surface morphology goes through the same trend with Sb coverage regardless of the

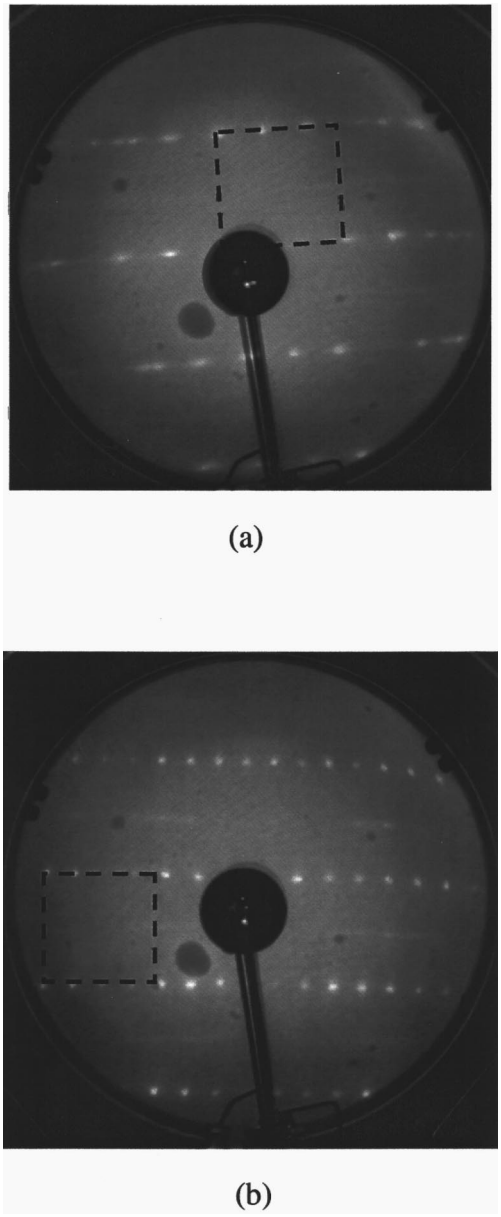

FIG. 3. Low-energy electron-diffraction patterns of (a) antimony-terminated and (b) clean, In-rich InP (001) surfaces. Electron energy=60 eV.

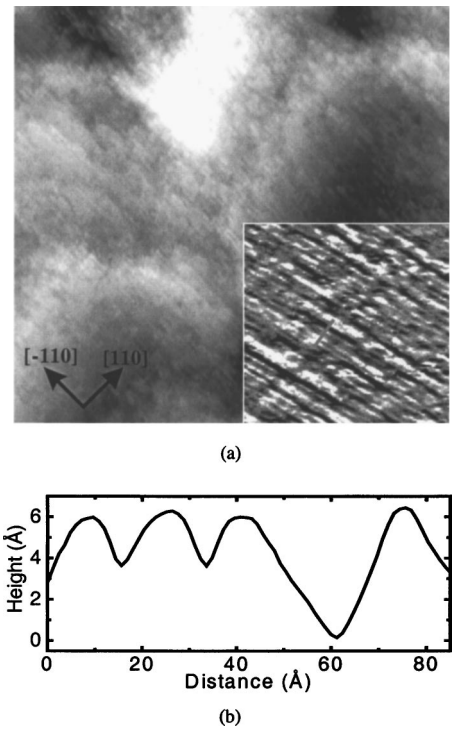

FIG. 4. (a) Scanning tunneling micrograph of the InP surface with 5.4 at. % Sb (image size=0.6×0.6 μm^2; inset=53×53 nm^2). (b) Topological scan of the straight line in the inset.

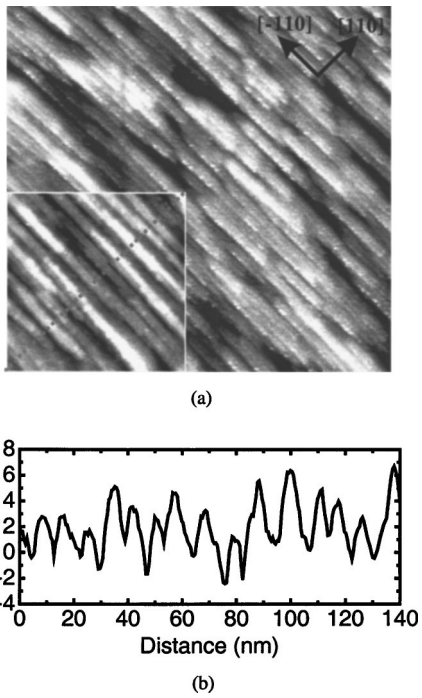

FIG. 5. (a) Scanning tunneling micrograph of the InP surface with 14.1 at. % Sb (image size=0.4×0.4 μm^2; inset=86×86 nm^2). (b) Topological scan of the dotted line in the inset.

treatment temperature. Surfaces with equivalent amounts of Sb exhibit identical scanning tunneling micrographs. This is consistent with the XPS results presented in Fig. 2, where the uptake of Sb in the film is independent of temperature and saturates at the same level.

Deposition of 5.4 at. % Sb on the InP surface significantly changes the structure, as can be seen in the STM image in Fig. 4(a). The step structure can still be discerned, but it has been smeared out by the incorporation of antimony. The terraces contain white ridges that are absent on clean InP (001). Shown in the inset of Fig. 4(a) is a picture that is 53×53 nm^2 in size. Here, one sees rows running along the [−110] crystal axis. The white, gray, and black ridges indicate that some rows are missing, while others have grown on top of the main terrace plane. The height scan across the line shown in the inset is presented in Fig. 4(b). It shows that the rows are 16.0 ± 0.5 Å apart, which corresponds to the length of four surface unit cells. This indicates that the $(2\times n)$ LEED pattern is derived from (2×4) surface unit cells. It is seen that the height difference between the black trenches and the white ridges is 6.0 Å, corresponding to two bilayers.

When 14.1 at. % Sb is deposited on the InP surface, it undergoes further changes, as shown in Fig. 5(a). The steps associated with the original terraces are no longer observed. Instead, the surface is covered with ridges or nanowires that extend long distances in the [−110] direction. The structure is further resolved in the small image in the lower left corner. The diagonal dotted line through this image is presented as a height scan in Fig. 5(b). This scan indicates that the ridges are 9.0 ± 2.0 nm in width, corresponding to 23 ± 4 surface unit cells, and for the most part, are either 3.0 or 6.0 Å in height, i.e., one to two bilayers. Due to the roughness of the surface, we were unable to achieve atomic-scale resolution.

The InP surface saturated with 22.0 at. % Sb is shown in Fig. 6(a). This surface is also terminated with a series of ridges of nanoscale dimensions that extend along the [−110] crystal axis. The inset shows a small image of 130×130 nm^2 in size. A height scan shown in Fig. 6(b) across

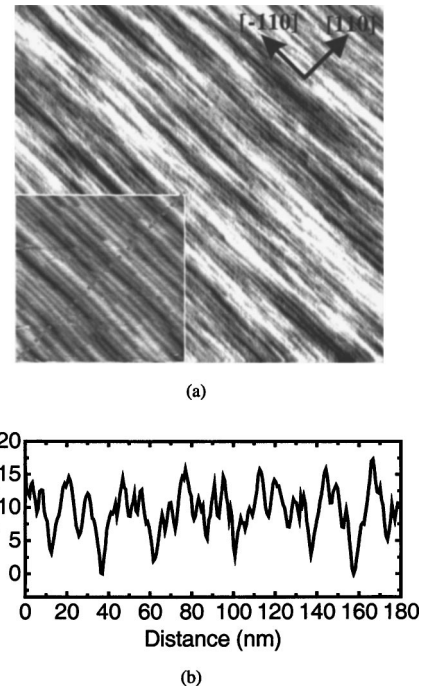

FIG. 6. (a) Scanning tunneling micrograph of the InP surface with 22.0 at. % Sb (image size=1.6×1.6 μm^2; inset=130×130 nm^2). (b) Topological scan of the dotted line in the inset.

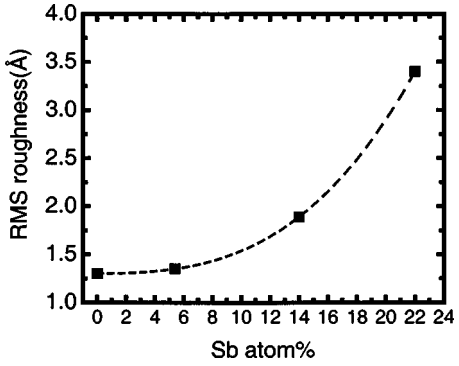

FIG. 7. The surface rms roughness along the [110] direction as a function of antimony uptake on InP (001).

the diagonal dotted line in the inset reveals that the surface corrugation has increased, resulting in a 12–18-Å change in height from the top of the ridges to the valleys. The deepest valleys are spaced ~25 nm apart. The ridges exhibit a sawtooth structure with smaller terraces that are 6.1 ± 2.0 nm wide and 5.8 ± 2.3 Å in height. These data demonstrate that the degree of faceting in the [110] direction increases as more antimony is deposited on the surface.

The root-mean-square (rms) roughness of the surfaces along the faceting direction has been calculated and is plotted in Fig. 7 versus the antimony uptake. The dashed line is a fit of a power-law function to the data, using an exponent equal to 3.0. These results show that the surface roughening accelerates with the Sb coverage.

We have found that if the MOVPE reactor was contaminated due to previous growth of GaAsSb films, then the InP surface would become covered with ~20 at. % Sb without introducing any TMSb into the process. This surface exhibited a sawtooth structure just like that shown in Fig. 6(a). Even though the reactor was contaminated with both arsenic and antimony, very little As was detected on the InP surface. The same trend of Sb and As contamination was observed by Wang *et al.* using time-resolved reflectance difference spectroscopy.[21] Baking the system at 700 °C for 1 h and coating the sample platter with InP only slightly decreased the antimony uptake on the InP film. In order to completely eliminate this contaminant, the platter had to be chemically etched, baked at 700 °C, and coated with InP.

IV. DISCUSSION

The constant Sb saturation level for TMSb exposure from 450 to 600 °C suggests that antimony desorption can be neglected, since the rate of this reaction would strongly depend on temperature through the Arrhenius relationship. Thus, antimony adsorption may be described by the following equation:[22]

$$\frac{d\theta_{\mathrm{Sb}}}{dt} = \frac{\frac{1}{4}\upsilon N_{\mathrm{TMSb}} S_0}{N}(2-\theta_{\mathrm{Sb}}), \tag{1}$$

where θ_{Sb} is the antimony coverage, ν is the mean molecular speed of TMSb molecules (m/s), S_0 is the initial sticking coefficient of TMSb on InP, N_{TMSb} is the number concentration of precursor molecules in the gas (m^{-3}), and N is the site concentration on InP (001), i.e., 5.8×10^{18} m^{-2}. This equation assumes that adsorption is rate limiting and follows a Langmuir isotherm with a saturation coverage of 2.0. Integrating Eq. (1) yields the following function for the antimony coverage:

$$\theta_{\mathrm{Sb}} = 2\left[1-\exp\left(-\frac{\frac{1}{4}\upsilon N_{\mathrm{TMSb}} S_0}{N}t\right)\right]. \tag{2}$$

The dotted line in Fig. 2 is the best fit of Eq. (2) to the data and it yields an initial sticking coefficient of $1.9\pm0.4\times10^{-4}$. This value is within the range of sticking coefficients observed for the adsorption of group-V precursors on compound semiconductor surfaces.[22]

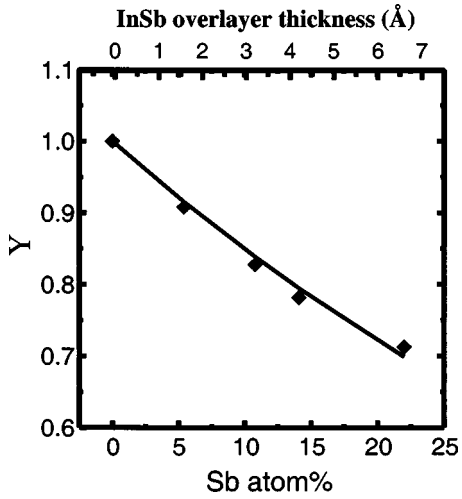

FIG. 8. The dependence of Y from Eq. (3) on the Sb uptake and the calculated InSb film thickness.

Since phosphorus and antimony atoms are so different in size with covalent radii of 1.00 and 1.45 Å, respectively, alloys of InPSb exhibit a large enthalpy of mixing.[23,24] This results in a miscibility gap with a critical temperature of 1319 K.[25] The region of immiscibility covers more than 95% of the solid composition range at temperatures from 450 to 600 °C.[25] Therefore, it is not surprising to observe a fixed uptake of antimony on indium phosphide without intermixing of the group-V elements.

The results presented above indicate that antimony displaces phosphorus from the topmost layers of the crystal, forming a skin of indium antimonide. The overlayer thickness, T, may be estimated from the P $2p$/In $3d$ peak intensity ratios using the following model:[26,27]

$$Y = \frac{(P2p/\ln 3d)\ \text{with Sb}}{(P2p/\ln 3d)\ \text{without Sb}} = \exp(-T/L). \tag{3}$$

This model assumes a uniform in-depth excitation, and an exponential decay in the intensity of the photoemission with $L=\lambda\cos\alpha$, where λ is the escape length of P $2p$ photoelectrons, equal to 22.0 Å,[28] and α is the takeoff angle, equal to 25°. Equation (3) indicates that the P/In ratio decays exponentially with the InSb thickness.

Figure 8 presents a plot of the left-hand side of Eq. (3) versus the antimony coverage, which is proportional to the InSb thickness.[29] The solid line in the figure is a least-

squares fit of the data to an exponential decay function, with an *R*-squared value of 0.99. The calculated overlayer thickness is shown on the upper *x* axis. For a saturation coverage of 22.0 at. % Sb, a thickness of 6.8 Å is obtained, which corresponds to two bilayers of InSb.

An asymmetric (1×3) LEED pattern has been reported for reconstructed InSb (001) surfaces.[30–32] Scanning tunneling micrographs indicate that the surface is covered with short, "wormlike" chains.[30] It has been suggested that this structure is composed of a mixture of several antimony-rich (2×4) reconstructions, resulting from the dimerization of the Sb atoms.[31,32] The exact positions of the *n* spots in the LEED are determined by the details of the sample preparation method. The $(2\times n)$ LEED pattern found in this work is consistent with the results reported in the literature, i.e., that the spacing between the diffraction spots varies in the [110] direction. In addition, the STM micrograph in Fig. 4(a) shows $\times4$ periodicity along the [110] axis, consistent with a (2×4)-like structure.

A large amount of strain must be accommodated by the epitaxial InSb film on InP, since the lattice constants of these materials differ by 10.4%.[33] The strain energy is released in the [110] direction by faceting, which accelerates with the thickness of the InSb layer, as seen in Fig. 7. By contrast, in the [−110] direction, elongated islands are formed most likely because the strain is relieved by dimer bond formation. The equilibrium Sb–Sb bond distance has been calculated to be 2.9 Å.[34,35] This is well short of the 4.0-Å spacing of the InP (001) lattice, and should be sufficient to counteract the tensile stress caused by the lattice mismatch.

V. CONCLUSIONS

We have investigated the decomposition of TMSb on InP in the MOVPE environment. For temperatures from 450 to 600 °C, a thin InSb film, ~6.8 Å thick, is deposited on the surface. The layer facets in the [110] direction due to lattice strain. This produces a sawtooth structure with ridges of 4–10 nm wide and a height corrugation in the facet direction of one to six bilayers. Evidently, Sb–Sb dimer bond formation relieves the strain in the [−110] direction, so that the film remains two dimensional (2D) along this axis.

ACKNOWLEDGMENTS

This research was supported in part by Northrop Grumman, Epichem, Emcore, and the University of California Discovery program, and in part by Sandia National Laboratories.

[1] M. Feng, N. Holonyak, B. Chu-Kung, G. Walter, and R. Chan, Appl. Phys. Lett. **84**, 4792 (2004).
[2] X. G. Xu, J. Hu, S. P. Watkins, N. Matine, M. W. Dvorak, and C. R. Bolognesi, Appl. Phys. Lett. **74**, 976 (1999).
[3] M. W. Dvorak, C. R. Bolognesi, O. J. Pitts, and S. P. Watkins, IEEE Electron Device Lett. **22**, 361 (2001).
[4] P. Soukiassian, P. S. Mangat, Y. Huttel, Z. Hurych, B. Gruzza, and A. Porte, J. Vac. Sci. Technol. B **11**, 1603 (1993).
[5] S. Abdellaoui, B. Gruzza, C. Pariset, M. Bouslama, C. Jardin, and D. Robert, Surf. Sci. Lett. **208**, L21 (1989).
[6] M. Yamada, A. M. Green, A. Herrera-Gomez, T. Kendelewicz, and W. E. Spicer, Appl. Phys. Lett. **59**, 3121 (1991).
[7] X. Yang, M. J. Jurkovic, J. B. Herox, and W. I. Wang, Appl. Phys. Lett. **75**, 178 (1999).
[8] X. Yang, J. B. Herox, M. J. Jurkovic, and W. I. Wang, Appl. Phys. Lett. **76**, 795 (2000).
[9] J. K. Shurtleff, R. T. Lee, C. M. Fetzer, and G. B. Stringfellow, Appl. Phys. Lett. **75**, 1914 (1999).
[10] R. M. Biefeld, Mater. Sci. Eng., R. **36**, 105 (2002).
[11] S. S. Yi, D. R. Chamberlin, G. Girolami, M. Juanitas, D. Bour, N. Moll, and R. Moon, J. Cryst. Growth **248**, 284 (2003).
[12] H. G. Liu, J. Q. Wu, N. Tao, A. V. Firth, E. M. Griswold, T. W. MacElwee, and C. R. Bolognesi, J. Cryst. Growth **267**, 592 (2004).
[13] A. Giani, F. Pascal-Delannoy, J. Camassel, and A. G. Norman, J. Mater. Sci. Lett. **20**, 677 (2001).
[14] J. Hu, X. G. Xu, J. A. Stotz, S. P. Watkins, A. E. Curzon, M. L. Thewalt, N. Matine, and C. R. Bolognesi, Appl. Phys. Lett. **73**, 2799 (1998).
[15] D. C. Law, Y. Sun, C. H. Li, S. B. Visbeck, G. Chen, and R. F. Hicks, Phys. Rev. B **66**, 045314 (2002).
[16] S. L. Zuo, Y. G. Hong, E. T. Yu, and J. F. Klem, J. Appl. Phys. **92**, 3761 (2002).
[17] C. A. Wang, D. A. Shiau, M. K. Connors, L. R. Danielson, G. Nichols, D. Donetsky, S. Anikeev, and G. Belenky, Mater. Res. Soc. Symp. Proc. **763**, 315 (2003).
[18] R. M. Biefeld, A. A. Allerman, S. R. Kurtz, and K. C. Baucom, J. Cryst. Growth **195**, 356 (1998).
[19] R. M. Biefeld, S. R. Kurtz, and A. A. Allerman, IEEE J. Sel. Top. Quantum Electron. **3**, 739 (1997).
[20] L. Li, B.-K. Han, Q. Fu, and R. F. Hicks, Phys. Rev. Lett. **82**, 1879 (1999).
[21] C. X. Wang, O. J. Pitts, and S. P. Watkins, J. Cryst. Growth **248**, 259 (2003).
[22] Y. Sun, D. C. Law, S. B. Visbeck, and R. F. Hicks, Surf. Sci. **513**, 256 (2002).
[23] J. C. Slater, J. Chem. Phys. **39**, 3199 (1964).
[24] G. B. Stringfellow, *Organometallic Vapor-Phase Epitaxy Theory and Practice*, 2nd ed. (Academic, San Diego, 1999).
[25] M. J. Jou, Y. T. Cherng, and G. B. Stringfellow, J. Appl. Phys. **64**, 1472 (1988).
[26] J. M. Moison, M. Bensoussan, and F. Houzay, Phys. Rev. B **34**, 2018 (1986).
[27] J. M. Moison, C. Guille, M. Van Rompay, F. Barthe, F. Houzay, and M. Bensoussan, Phys. Rev. B **39**, 1772 (1989).
[28] P. J. Cumpson and M. P. Seah, Surf. Interface Anal. **25**, 430 (1997).
[29] D. C. Law, Y. Sun, and R. F. Hicks, J. Appl. Phys. **94**, 6175 (2003).
[30] C. F. McConville, T. S. Jones, F. M. Leibsle, S. M. Driver, T. C. Q. Noakes, M. O. Schweitzer, and N. V. Richardson, Phys. Rev. B **50**, 14965 (1994).
[31] W. K. Liu and M. B. Santos, Surf. Sci. **319**, 172 (1994).
[32] A. G. de Oliveira, S. D. Parker, R. Droopad, and B. A. Joyce, Surf. Sci. **227**, 150 (1990).
[33] *Handbook Series on Semiconductor Parameters*, Vol. 2, edited by M. Levinstein, S. Rumyantsev, and M. Shur (World Scientific, London, 1996).
[34] W. G. Schmidt, Appl. Phys. A: Mater. Sci. Process. **65**, 581 (1997).
[35] W. G. Schmidt and F. Bechstedt, Phys. Rev. B **54**, 16742 (1996).